

Resolution of 90 nm ($\lambda/5$) in an optical transmission microscope with an annular condenser

Arnold Vainrub, Oleg Pustovyy, and Vitaly Vodyanoy

Department of Anatomy, Physiology and Pharmacology, College of Veterinary Medicine, Auburn University, Auburn, Alabama 36849

Received June 12, 2006; accepted July 18, 2006;
posted July 26, 2006 (Doc. ID 71923); published September 11, 2006

Resolution of 90 nm was achieved with a research microscope simply by replacing the standard bright-field condenser with a homebuilt illumination system with a cardioid annular condenser. Diffraction gratings with 100 nm width lines as well as less than 100 nm size features of different-shaped objects were clearly visible on a calibrated microscope test slide. The resolution increase results from a known narrower diffraction pattern in coherent illumination for the annular aperture compared with the circular aperture. This explanation is supported by an excellent accord of calculated and measured diffraction patterns for a 50 nm radius disk. © 2006 Optical Society of America

OCIS codes: 170.0180, 050.1940, 110.1220, 100.6640.

Recent progress in high-resolution optical microscopy (reviewed in Refs. 1 and 2) has been boosted by the demands of cellular biology and nanoscience. In fluorescence microscopy image resolution of a few tens of nanometers was demonstrated.^{3,4} However, in transmission and reflection microscopy with visible light illumination, even for modern confocal instruments the reported lateral image resolution does not surpass 180 nm.^{1,2,5} In this Letter we report 90 nm resolution in the images obtained using an optical illumination system with a high-aperture cardioid annular condenser (annular A-condenser). The system produces a highly oblique hollow cone of light (N.A. = 1.2–1.4). Coupled with a high-aperture microscope objective with an iris, the system provides two different regimes of illumination (Fig. 1). When the iris is closed so that no direct light enters the objective after passing through the object, only refracted, scattered, or diffracted light goes in the objective (Fig. 1a, dark-field illumination). If the iris is open in such a way as to allow the direct entrance of light into the objective, the front lens of the objective is illuminated by the annular light produced by the empty cone of light entering the objective (Fig. 1b, bright-field illumination). The cardioid condenser⁶ is an integral part of the illumination system, so the system comprises collimation lenses and a first surface mirror that focus light onto the annular entrance slit of the condenser. As part of the illumination system, the condenser is prealigned, and therefore additional alignment is unnecessary. The illumination system is positioned in an Olympus BX51 microscope by replacing a regular bright-field condenser (circular C-condenser). The illumination system is connected with a light source (EXFO120, Photonic Solution) by a liquid light guide. The objective used for this work is an infinity-corrected objective HCX PL APO 100 \times /1.40–0.70, oil, iris from Leica. The image is magnified with a zoom intermediate lens (2 \times -U-CA, Olympus), a homebuilt 40 \times relay lens, and captured by a Peltier-cooled camera (AxioCam HRc, Zeiss) and a Dimen-

sion 8200 Dell computer. The microscope is placed on a vibration-isolation platform (manufactured by TMS). Bright-field images were obtained by replacing the illumination system with an Olympus bright-field condenser (N.A. 1.4/0.9) and connecting the EXFO120 light source with the rear microscope light port by an Olympus X-Cite120 adaptor. All images were made using Richardson test slides.⁷ The geometrical patterns that were chosen for imaging include vertical grating arrays that provide a series of lines of 100 nm width at a 200 nm period, vertical/horizontal resolution bar sets, a star pattern, different-shaped patterns, and solid circles. Patterns of Richardson slides were tested with a JEOL 7000F field emission scanning electron microscope. Scales were calibrated by a NIST traceable master system (Hewlett-Packard Dynamic Calibrator Model HP5529A). Figure 2 shows high-resolution images obtained from the Richardson slide high-resolution patterns. The practical resolution estimated from the images is $\lambda_0/5$.

To understand the enhanced resolving power, we present the diffraction theory of optical image results for both the cases of C- and A-illumination systems (C-circular, A-annular). For simplicity, the calculations are performed for the axial symmetry case of an

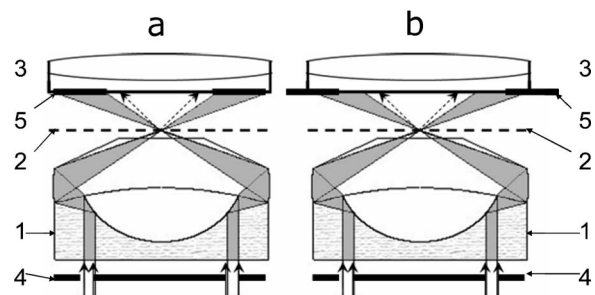


Fig. 1. Cardioid annular condenser (A-condenser). The illumination regime is installed by the iris opening: a, dark-field; b, bright field. 1, condenser; 2, sample; 3, objective; 4, annular diaphragm; 5, iris.

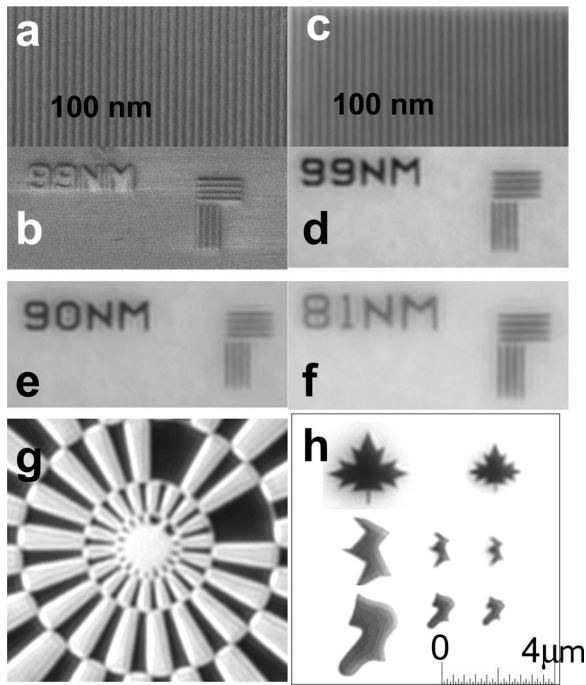


Fig. 2. Images of Richardson slide patterns: a, b, scanning electron microscope images; c–h, optical images obtained with the A-condenser. c–f, 100, 99, 90, and 81 nm imaged with 10 nm band filters of 500, 500, 450, and 405 nm, respectively; g, star pattern with 36 sectors, with a 546 nm filter [at the smallest central circle ($r=650$ nm) the arcs are ~ 110 nm]; h, various shape patterns, with a 546 nm filter. Top row of h, maple leaf patterns with stem widths of (left) 102 and (right) 71 nm; middle and bottom rows, sharp and round-edged shapes; the scale bar of $4 \mu\text{m}$ is for h only.

opaque disk of radius $r=50$ nm when the image is given by compact integrals that are easy to evaluate. In addition, the small object's size compared with the light wavelength used, $\lambda_0=546$ nm, ensures totally coherent illumination conditions. Experimentally, we measured images of a 50 nm radius disk (chromium film circle on a glass Richardson slide) for different microscope objective N.A. in the range 0.7–1.4. As we show, the theory is in excellent accord with the experiment and thus clearly reveals the mechanism of improved resolution.

The light amplitude $U_1(x_1, y_1)$ in the image formed by a coherent optical system can be written as the convolution of the input in object's plane $U_0(x_0, y_0)$ and the point spread function (PSF) $P(x, y)$ (Chap. 9 of Ref. 8):

$$U_1(x_1, y_1) = \int_{-\infty}^{\infty} \int_{-\infty}^{\infty} U_0(x_0, y_0) P(x_1 - x_0, y_1 - y_0) dx_0 dy_0. \quad (1)$$

First, we consider the bright-field regime. The C-condenser forms a light cone with N.A. = 1.4 that fills up all the pupil. For A-condenser the hollow light cone with N.A. = 1.2–1.4 illuminates only the corresponding peripheral ring of the entrance pupil (Fig. 1b). Therefore, in the pupil of radius a with aperture N.A. = 1.4 the inner and outer radii of the illuminated

ring are ϵa and a , respectively, where $\epsilon=1.2/1.4=0.86$ (an entrance aperture less than N.A. = 1.2 corresponds to the dark-field regime and is considered separately below). Omitting the derivation (to be published in the future), from Eq. (1), we get the image of the circular hole of radius r on the opaque screen:

$$U_1(\rho_1) = \frac{k_0 N r}{a} \int_{\epsilon a}^a J_1\left(\frac{k_0 N r \rho}{a}\right) J_0\left(\frac{k_0 N \rho_1 \rho}{a}\right) d\rho. \quad (2)$$

Here ρ_1 is the radius in the image plane, N is numerical aperture, $J_0(x)$ and $J_1(x)$ are the Bessel functions, and $k_0=2\pi/\lambda_0$, where λ_0 is the light wavelength in vacuum. This result was derived for $\epsilon=0$ (C-condenser) by Martin (Chap. 6 of Ref. 9) and Hopkins,¹⁰ and we generalize it here for the A-condenser in bright-field mode ($0 < \epsilon \leq 1$). We computed the integral in Eq. (2) using Mathematica 5 software (Wolfram Research). Finally, applying Babinet's principle (Chap. 11 of Ref. 8.), we get for the image of opaque circular disk

$$U_d(\rho_1) = U - U_1(\rho_1). \quad (3)$$

Here U is the amplitude without any object, which in our case is constant because of the small size of the disk, $r=50$ nm. In the experiment we measure the intensity $I_d(\rho_1)=|U_d(\rho_1)|^2$.

Next we briefly consider the dark-field regime (Fig. 1a). For our A-condenser this occurs when the iris diaphragm reduces the entrance N.A. to < 1.2 . To describe the light wave scattered by the chromium disk, we follow the directions of Mie theory for diffraction by a conducting sphere (Chap. 14 of Ref. 8). For the sphere's radius $r < \lambda_0$, the scattering diagram $u_0(\xi)$ is strongly anisotropic with the maxima along the incident light beam $\xi=0$, where ξ is the scattering angle. We model it as

$$u_0(\xi) = \cos^m \xi, \quad (4)$$

shown in Fig. 3a. Equation (4) was integrated in close form (not shown) over all radial directions in the hollow cone of incident light. The resulting light distribution in the entrance aperture for m values of 2, 6, and 12 is shown in Fig. 3b. Remarkably, it is an annular-type pattern with the minimum in the center and an increase of light concentration on the pe-

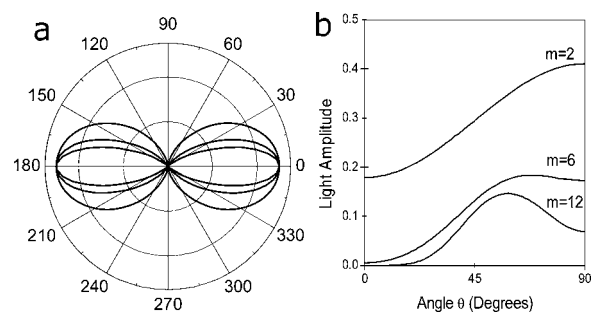


Fig. 3. a, Scattering diagram of Eq. (4) for $m=2$ (outer), $m=6$ (middle), and $m=12$ (inner). b, Polar angle distribution of the scattered light amplitude over the objective lens aperture in the dark-field regime of the A-condenser.

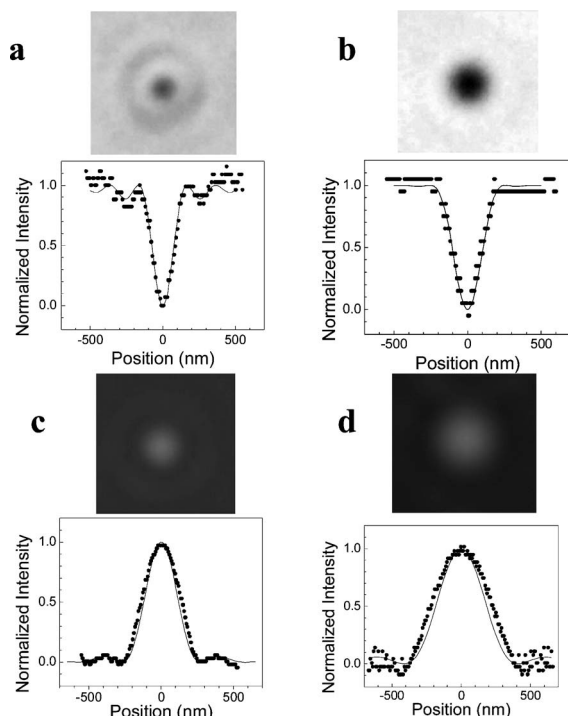


Fig. 4. Images and intensity plots of 50 nm radius opaque disk. Bright-field images: a, cardioid condenser, N.A.=1.4; b, Olympus condenser, N.A.=1.4. Dark-field images: cardioid condenser, c, N.A.=1.1; d, N.A.=0.7. Dots, experiment; solid curves, theory.

riphery as m increases. Further, the PSF was calculated and the image in dark-field regime was evaluated using Eq. (1). The theory's details will be published elsewhere.

Now we compare the theory with experiment. In the bright field the calculation does not involve any fitting parameters because all the values in Eq. (2) are known and listed in the text above. Figures 4(a) and 4(b) demonstrate an excellent agreement between theory and experiment for both the C- and the A-condensers. In particular, for the A-condenser the theory describes accurately the shape of the central minima as well as the position and height of the first diffraction ring (Fig. 4a). In the dark field the theory is also in perfect accord with the experiment, as shown in Figs. 4(c) and 4(d). The fittings define the only unknown parameter in Eq. (4) as $m=6$.

It is interesting to consider the results in Fig. 4 from the point of view of the Rayleigh criterion that predicts $R=0.61(\lambda_0/N)=238$ nm. As is known, R is the radius of the first dark ring in the Airy pattern for an isotropic lighting point source and a circular entrance aperture. Experimentally, for the C-condenser the radius is 260 nm (Fig. 4b), slightly above $R=238$ nm as expected because of the finite size $r=50$ nm of the imaged disk. Remarkably, for the A-condenser the observed radius of 165 nm (Fig. 4a) is $(238/165)=1.44$ times smaller than R . Indeed, this is not a surprise but is consistent with known nar-

rowing of the central spot in diffraction pattern when the entrance aperture is annular (Chap. 8 of Ref. 8) because the A-condenser in the bright-field regime illuminates only the peripheral ring on the entrance pupil. Similar but smaller narrowing is observed in the dark-field images in Fig. 4, where the measured radii of darkness are 270 nm at $N=1.1$ and 420 nm at $N=0.7, 1.1,$ and 1.15 times less than the Rayleigh criterion values, respectively. Again, this results from an annularlike distribution of scattered light over the entrance pupil, as shown in Fig. 3b.

The practical resolution with the annular A-condenser in the bright field that is demonstrated in Fig. 2 is better than $\lambda_0/5$. This surpasses by 2.2 times the Rayleigh criterion $R=\lambda_0/2.3$ for the N.A. that was used, 1.4. The presented theory explains the enhanced image resolution as having two reasons. First, the PSF is narrower for an annular A-condenser. Second, for the A-condenser the diffraction fringes of the PSF are strong (Fig. 4a) and subsequently change the phase by π . Hence PSF convolution with the object's shape in Eq. (1) smears the image edges less; the effect appears only for coherent illumination.

In conclusion, we have reported $\lambda_0/5$, or better than 90 nm, resolution in imaging with a standard research transmission optical microscope modified only by using a homebuilt illumination system with a cardioid annular condenser. This resolving power is achieved in visual observation or CCD camera recording without any image postprocessing. In addition to the reported data, we observed high resolution in real-time imaging of live cells. Our calculations show that enhanced resolution is in complete accord with the classical diffraction theory of imaging systems and results from high-aperture coherent annular illumination.

This research was supported by the U.S. Department of Defense (grant DAAD 05-02-C-0016), the John E. Fetzer Institute, Inc. (grant 2143), and Aetos Technologies, Inc. V. Vodyanoy's e-mail address is vodyavi@auburn.edu.

References

1. S. W. Hell, *Nat. Biotechnol.* **21**, 1347 (2003).
2. Y. Garini, B. J. Vermolen, and I. T. Young, *Curr. Opin. Biotechnol.* **16**, 3 (2005).
3. V. Westphal and S. W. Hell, *Phys. Rev. Lett.* **94**, 143903 (2005).
4. M. G. L. Gustafsson, *Proc. Natl. Acad. Sci. U.S.A.* **102**, 13081 (2005).
5. M. Schrader, M. Kozubek, S. W. Hell, and T. Wilson, *Opt. Lett.* **22**, 436 (1997).
6. L. C. Martin, *An Introduction to Applied Optics*, Vol. 2 (Pitman & Sons, 1932).
7. T. M. Richardson, *Proc. R. Microsc. Soc.* **33**, 3 (1998).
8. M. Born and E. Wolf, *Principles of Optics*, 7th ed. (Cambridge U. Press, 1999).
9. L. C. Martin, *The Theory of the Microscope* (Elsevier, 1966).
10. H. H. Hopkins, *Sci. J. R. College* **20**, 100 (1949).